Bioorganic Chemistry 85 (2019) 117–127

Contents lists available at ScienceDirect

Bioorganic Chemistry

journal homepage: www.elsevier.com/locate/bioorg

Expansion of the scaffold diversity for the development of highly selective butyrylcholinesterase (BChE) inhibitors: Discovery of new hits through the pharmacophore model generation, virtual screening and molecular dynamics simulation

Xin Lu[a], Hongyu Yang[a], Qihang Li[a], Yao Chen[b], Qi Li[a], You Zhou[c], Feng Feng[d], Wenyuan Liu[e], Qinglong Guo[f], Haopeng Sun[a,*]

[a] Department of Medicinal Chemistry, China Pharmaceutical University, Nanjing 211198, People's Republic of China
[b] School of Pharmacy, Nanjing University of Chinese Medicine, Nanjing 210023, People's Republic of China
[c] College of Biotechnology, Southwest University, Chongqing 400715, People's Republic of China
[d] Department of Natural Medicinal Chemistry, China Pharmaceutical University, Nanjing 211198, People's Republic of China
[e] Department of Analytical Chemistry, China Pharmaceutical University, Nanjing 210009, People's Republic of China
[f] State Key Laboratory of Natural Medicines, Jiangsu Key Laboratory of Carcinogenesis and Intervention, School of Basic Medicine and Clinical Pharmacy, China Pharmaceutical University, Nanjing 210009, People's Republic of China

ARTICLE INFO

Keywords:
Selective butyrylcholinesterase
Pharmacophore modeling
Virtual screening
Molecular dynamics
Alzheimer's disease

ABSTRACT

Butyrylcholinesterase (BChE) is recently considered as a new target for the treatment of Alzheimer's disease (AD). There is an increasing interest in the development of BChE inhibitors. In the present study, a set of pharmacophore models for BChE was developed and validated. Based on the models, virtual screening was performed on five compound collections, from which seventeen potential hits were retained for biological investigation. In total, eight of these seventeen potential hits showed selective BChE inhibitory activity. Moreover, four compounds displayed IC_{50} values in sub-micromolar range on *eq*BChE and three displayed IC_{50} values $< 2\,\mu M$ on huBChE. The diverse scaffolds of the active compounds provided good starting point further development of selective BChE inhibitors. As far as we concerned, here we disclose the first selective pharmacophore model targeting BChE. The high rate of the model in the identification of active hits indicates it is a valuable tool for the development of selective BChE inhibitors, which may benefit the treatment of AD.

1. Introduction

Alzheimer's disease (AD), the most common form of dementia, accounts for 50–75% of all cases [1]. The prevalence of dementia shows an almost exponential increase with age. It is higher than 24% in people aged 85 years or older in the Western world [2]. Until now, no therapies or drugs were able to slow or reverse the course of the disease. Huge number of patients and heavy financial burden make it one of the great challenges of human health and social issues [3]. The memory and cognitive impairment are the major symptoms associated with dementia, and it is mainly due to the loss of neurotransmitter cholinesterase from the neurons of the central nervous system [4–6]. Cholinergic dysfunction is one of the main pathological hallmarks of AD [7]. Mainly, two types of cholinesterase enzyme, namely acetylcholinesterase (AChE) and butyrylcholinesterase (BChE), take charge of hydrolyzing the acetylcholine (ACh) in human [8]. AChE has long been considered as a key target for regulating the activity of the cholinergic system in view of that ACh is mainly hydrolyzed by AChE under normal conditions. However, experimental evidence demonstrated the significant role of BChE during disease onset and progression, especially in the AChE-deficient brains of AD patients [9]. Indeed, AChE activity in the brain of AD patients declines while BChE activity remains unchanged or increases. This makes the role of BChE as Ach-hydrolyzing enzyme progressively increasing during the disease evolution [10]. Furthermore, BChE knockout mice showed no physiological disadvantage, and silent BChE mutations in humans showed a slower rate of cognitive decline [11]. Hence, it is expected that inhibiting BChE could benefit AD patients the same way AChE inhibition does. Experiment *in vivo* supported this hypothesis that specific BChE inhibitors were able to restore ACh levels in mice and improve the cognitive

* Corresponding author.
E-mail address: sunhaopeng@163.com (H. Sun).

https://doi.org/10.1016/j.bioorg.2018.12.023
Received 12 November 2018; Received in revised form 29 November 2018; Accepted 17 December 2018
Available online 21 December 2018

impairment caused by the amyloid-β peptide, yet without peripheral adverse side effects, which are known to be the defect of traditional AChE inhibitors [12].

Besides, BChE is also found to correlate positively with the formation of plaques and neurofibrillary tangles (NFTs) in human AD brain tissue as well as in plaques in AD mouse models [13]. In 5XFAD mouse model, BChE knockout mice diminished deposition of fibrillar Aβ in AD [14]. It has been suggested that BChE could play a noticeable role in the transformation of Aβ from an initially benign form to an ultimately malignant form of amyloid plaques causing brain tissue degeneration and clinical dementia in disorders [15]. A research recently published highlighted the predictive value of BChE as a biomarker for timely diagnosis of AD [16]. In summary, selective BChE inhibitors could be of importance for treatment of AD and exploration of the pathogenesis of AD.

Up to now, only a few selective BChE inhibitors were reported, such as heterobivalent tacrine derivatives [17], benzofurans [18], isosorbide-based compounds [19], cymserine analogs [20] and naphthamide compounds [21]. There is currently an urgent call for the discovery of selective BChE inhibitors. In this paper, we described the construction of a structure-based pharmacophore model which leaded to the discovery of several BChE inhibitors. A highly selective BChE inhibitor with naphthoquinone amide group (Fig. 1) was chosen as the temple. Starting from the complex of BChE and **1** (PDB: 5DYW), we created and validated several pharmacophore hypotheses. The one with best performance was used as three-dimension (3D) entry to search several commercial databases. Docking stimulation and clustering helped us choose 17 compounds for bioassays. The employed screening workflow that had allowed us to identify selective BChE compounds was depicted in Fig. 2. Finally, 8 compounds with diverse scaffolds were identified as selective BChE compounds. The discovery of new emerging molecules with different structural skeletons enriched the structural types of highly selective BChE inhibitors and provided lead compounds for the subsequent optimization for medicinal chemists.

2. Results and discussion

2.1. Pharmacophore model generation

The pharmacophore model was generated by using Discovery Studio 3.0 (DS). The 3D structure of BChE bound with compound **1** was chosen as input. By means of this automated structure-based model generation, we obtained ten 3D pharmacophore hypotheses representing the main interactions.

The reliability of the SBP (i.e. ability to discriminate between inhibitors and non-inhibitors) was assessed and improved using a dataset of 10 active compounds (Fig. S1) retrieved from Chembl or documents and 360 decoys. The actives were chosen based on following criterias: BChE IC_{50} < 1 μM and SI (BChE IC_{50}/AChE IC_{50}) > 10. The decoys were generated by DecoyFinder tool (http://URVnutrigenomica-CTNS.github.com/DecoyFinder) [22]. DecoyFinder tool, disclosed in 2012, is an easy-to-use python GUI for building target-specific decoys set [23]. The principle of selecting decoys is based on that their similarity to active ligands according to five physical descriptors (molecular weight, number of rotational bonds, total hydrogen bond donors, total hydrogen bond acceptors and the octanol–water partition coefficient). In the case of the decoy set, all compounds were prepared retaining the chirality and then were minimized in DS. Multi-conformational screening of these compounds was carried out and the signal-noise ratio was determined using a receiver operating characteristics (ROC) curve (Table1, Fig. S2). The model (Hypo_07) exhibited an excellent sensitivity in retrieving 89% (16 out of 18) of the active compounds (Fig. 3A).

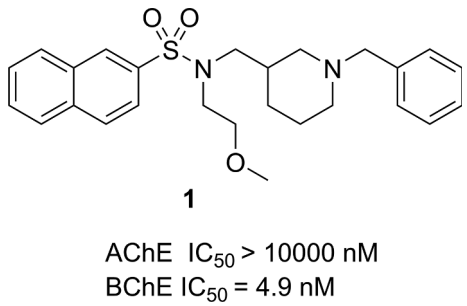

Fig. 1. The structure of naphthoquinone amide.

The chemical features of the final model mainly represent ligand-enzyme interactions detected at the center of the catalytic cavity. This model consists of one positive ionizable interaction (PI) and one hydrophobic contact (HYD) with Tyr332, one HYD with Ph329, Leu286, and Trp231; two H-bond acceptor (HBA) with Thr120, and one ring-aromatic (RA) with Trp82 (Fig. 3B). Exclusion volumes were defined as forbidden areas to represent the steric constraints of the pocket.

2.2. Virtual screening

After validation of the 3D pharmacophore, the model was used for virtual screening of six commercial compound collections: Chemdiv (915527), DruglikeDiverse (5384), Enamine (2188917), Interbioscreen (547040), PPi (25000), Speces (212221). Compounds passed the pharmacophore filter were ranked using the pharmacophore fit value and only the compounds whose fit value > 3 were retained.

In order to reduce the amount of compounds to handle prior to biological investigation, druglike descriptors, docking and structural clustering were utilized. Firstly, druglike descriptors of Lipinski and veber rules helped discarding the compounds with unfavorable physicochemical properties. Then, the CDOCKER module of DS was used to dock all selected virtual hits into the BChE active site (PDB code 5DYW) to check that their interactions in the binding site of BChE. We focused on checking whether the compounds interacted with Trp82 which is an important amino acid of BChE. Furthermore, 463 compounds retained were subjected to structural clustering within Cluster Ligand module of DS. These compounds were divided into 10 clusters by fingerprint and the top ten in each cluster were chosen for visual inspection. Considering the binding mode and structural diversity, seventeen candidates (Fig. 4) were selected and purchased from Topscience (www.tsbiochem.com) for biological determination.

2.3. Biological evaluation

Seventeen compounds have been first evaluated for their ability to inhibit BChE from equine serum (*eq*BChE) and AChE from electrophorus electricus (*ee*AChE) at a concentration of 10 μM. This preliminary assay resulted in eight hits which exhibited over 50.0% inhibitory effects on BChE (Fig. 5). Most interestingly, all these showed no more than 30% inhibitory against AChE at the concentration 10 μM. The results demonstrated that the eight compounds were selective BChE inhibitors. They were subsequently assayed for dose-dependent inhibitory activity against *eq*BChE (Fig. 6A), and their IC_{50} values were calculated (Table 2). Eight compounds showed inhibitory on BChE range from 0.3 ± 0.1 μM ~ 13.5 ± 2.2 μM while four compounds (**2**, **5**, **11** and **13**) showed micro-molar inhibitory activity (0.6 ± 0.2 μM, 0.3 ± 0.1 μM, 0.7 ± 0.2 μM, 0.7 ± 0.2 μM, respectively). Furthermore, the dose-dependent inhibitory activity of eight hit compounds against BChE from human (huBChE) (Fig. 6B) was performed. The IC_{50} of four compounds (**10**, **11**, **13** and **17**) on huBChE was equivalent to that of *eq*BChE while the others were far worse. The two most potent compounds (**11** and **13**) showed the IC_{50} on huBChE of 1.3 ± 0.6 μM and 1.4 ± 1.9 μM. The results require further verification to eliminate interference of accidental factors. Even so, these compounds provide a variety of structural types available for subsequent optimization.

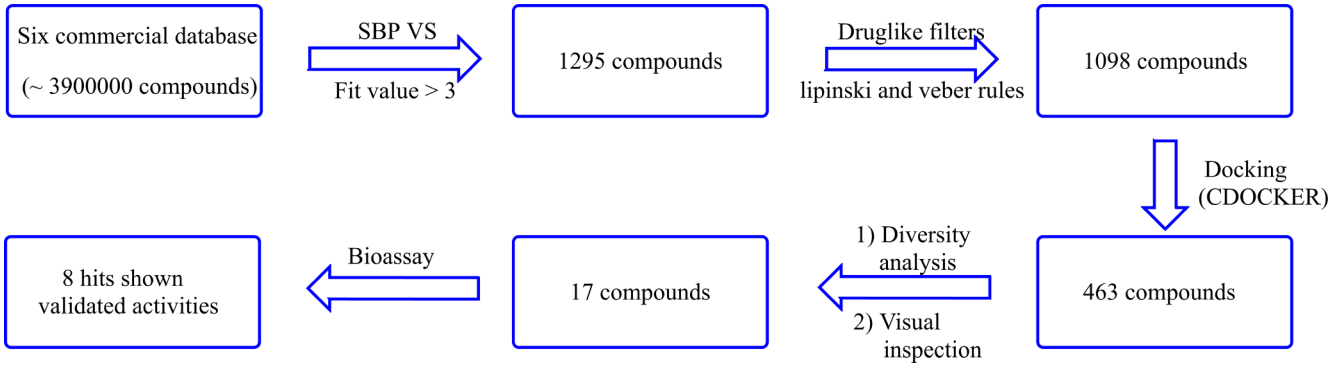

Fig. 2. Overall workflow of the screening procedure. The six commercial databases were Chemdiv, DruglikeDiverse, Enamine, Interbioscreen, PPi and Speces.

Table 1
Statistical parameters for validation of hypo-07.

Parameters	Values
Total positives	18
Total negatives	515
True positives	16
True negatives	279
False positives	236
False negatives	2
Sensitivity	0.89
Specificity	0.54
ROC	0.81

2.4. Kinetic studies

To gain more information on the mechanism of the inhibitory of BChE, four compounds (**10, 11 13** and **17**) were selected to perform kinetic studies with BChE by Lineweaver-Burk reciprocal plots as described previously. Generally, Lineweaver-Burk plots can be described by reciprocal rates versus reciprocal substrate concentrations for different inhibitor concentrations resulting from the substrate-velocity curves for BChE. Besides, kinetic studies of compounds **2** and **5** were also analyzed. We did not consider them in the follow-up evaluation because of the big differences between their activities against *eq*BChE and huBChE. The enzyme kinetic data of these two compounds are placed in Fig. S3.

For all four compounds, the Lineweaver-Burk plot showed increased slopes (increased V_{max}) and invariable intercepts (fixed K_m) at increasing concentrations of the inhibitors (Fig. 6A, B, C and D), leading to a competitive inhibitory pattern. It indicates that all compounds may bind to catalytic “anionic” site (CAS) when interacting with BChE.

2.5. Docking stimulation of hit compounds

Detailed binding patterns of the four compounds (**10**, **11**, **13** and **17**) to BChE were investigated by the CDOCKER module in DS. Generally, these compounds bound to BChE in similar U-shaped conformations. In detail, for **10** (Fig. 7A), the benzene group was inserted into the bottom of the acyl pocket and formed hydrophobic contacts with Trp82, which are key residue in the CAS of BChE. Furthermore, the furan group formed with Gly116 Trp231 and Leu286. The 3,4-dihydroquinazolin group interacted with Tyr332 by π-π T-shaped. Besides, the protonated N atom of piperazine can form salt bridge with Asp70, which further enhanced the inhibitory.

For **11** (Fig. 7B), the benzyl moiety inserted into the CAS of BChE and interacted with Tyr82. The 3,4-dimethylbenzene group provides π-π T-shaped with Trp329 and Gly116, while formed several π-alkyl interactions with Trp231 and His438. The piperazine ring formed a π-

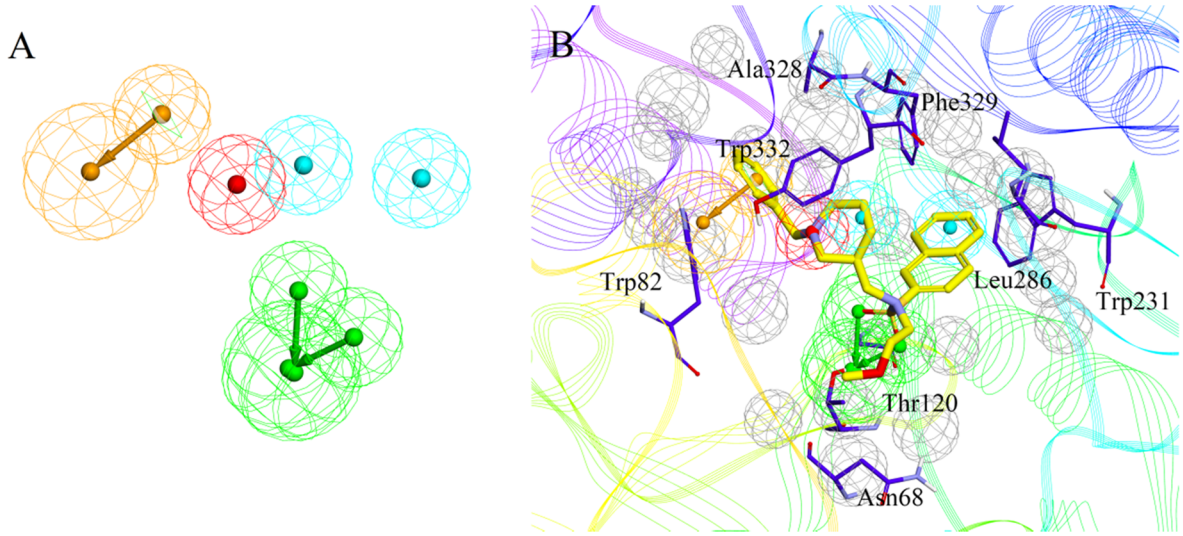

Fig. 3. (A) The pharmacophore model of hypo-07, to better elucidate the model, the excluded volume was deleted. (B) The pharmacophore model bound with complex. The compound is shown in yellow stick mode. Key residues of BChE are depicted in blue thin stick mode. Only polar hydrogen atoms are shown. In the pharmacophore model, the hydrogen bond acceptor, cation, aromatic ring, hydrophobic portion and excluded volumes are colored green, red, orange and gray, respectively.

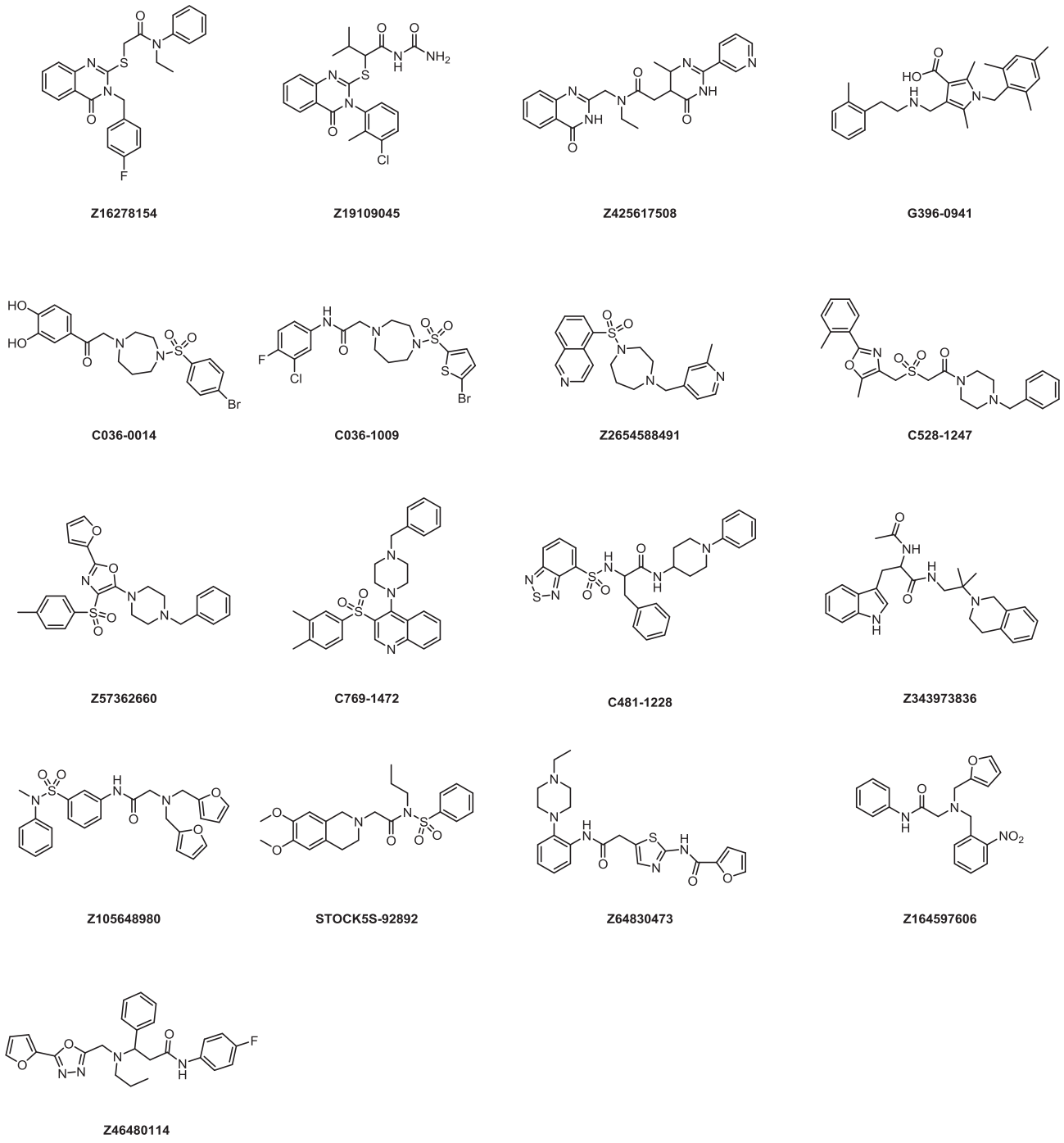

Fig. 4. Chemical structure of compounds selected for *in vitro* tests.

alkyl interaction with Tyr332. The additional H-bonds with Pro285 further improved activity.

For **13** (Fig. 7C), the positively charged tetrahydroisoquinoline nitrogen formed attractive charge with Asp70 in peripheral site. The benzene group of tetrahydroisoquinoline moiety interacted with Trp82 *via* π-π T-shaped. The 1H-Indole created π-π *T*-shaped with Trp329 and amide-π stacked with Gly116. Though acetyl and methyl groups on the side chain did not formed any interactions with protein, they stabilized the U-shaped conformation. This may explain why compound **13** has high selectivity on AChE.

For **17** (Fig. 7D), the unsubstituted benzyl inserted into the CAS and formed hydrophobic interactions with Trp82 and Ala328. The nitrobenzene group formed π-π stacked with Tyr332. Furthermore, the protonated tertiary amine formed attractive charge with Asp70 in peripheral site.

As told above, we can summarize that four compounds interacted with CAS such as Trp82. The results of docking studies were consistent with the results of enzyme kinetics.

2.6. Molecular dynamics

To evaluate the stability of each system of BChE in complex with small molecules, molecular dynamics simulations were conducted in Amber. The docking poses of **10**, **11**, **13** and **17** with BChE underwent 100 ns. MD simulations and stable MD simulations trajectories were utilized for data extracting and binding free energy calculating. The

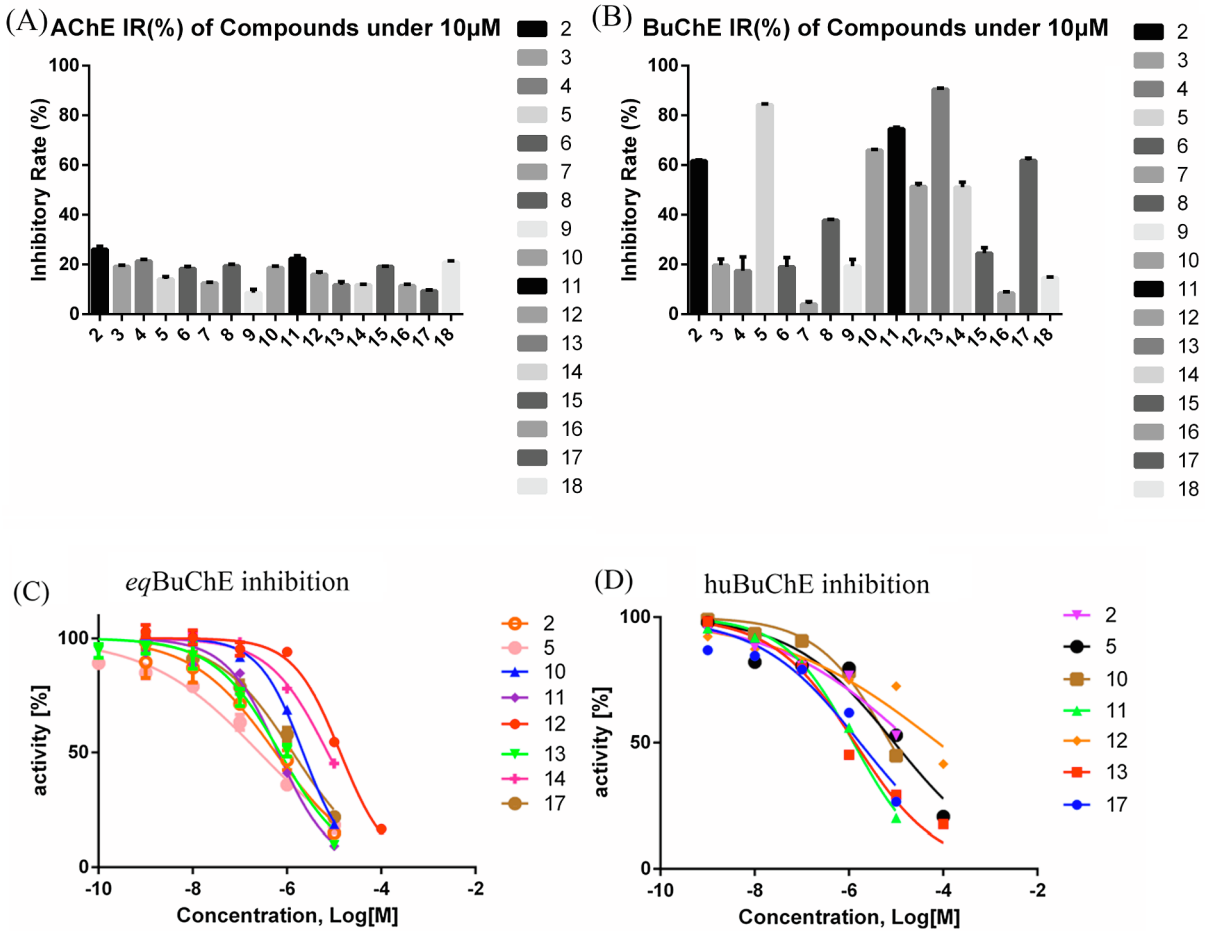

Fig. 5. ChEs IR(%) of hit compounds under 10 μM (A and B); IC_{50} curves of eight hits against *eq*BChE (C) and huBChE (D), respectively.

root-mean-squared deviation (RMSD) values of the protease backbone atoms during the MD simulation relative to their crystal structures were provided in Fig. S4. The total binding free energy of **10**, **11**, **13** and **17** was calculated with the MM-PBSA method (Table 3). The total binding free energy was −50.45, −53.00, −36.29 and −29.04 kcal/mol for the complexes of BChE-**10**, BChE-**11**, BChE-**13** and BChE-**17**, respectively, in agreement with the IC_{50} except **10**. As the docking studies demonstrated, the p-methylbenzoyl group played role of forming the U-shaped conformation for better protein bound, which may explain the higher binding free energy.

Residue contributions of potential hot residues were also performed to evaluate the contribution of residues in the binding pocket of BChE with the MM-PBSA method. Meanwhile, energy decomposition of potential hot residues was performed to explore which interactions dominated in the binding free energy. Usually, a residue is considered to be important for recognition of ligands if the interaction energy with ligand is lower than −1 kcal/mol [24]. For **10** (Fig. 8A), the results suggest that the residues may be important for inhibition of **10** on BChE: Trp82 (−1.01 kcal/mol), Trp231 (−1.55 kcal/mol), Phe329 (−2.53 kcal/mol). Among these residues, Phe329 mostly contributed to the total binding free energies. The interaction with Asp70 in the PAS (0.65 kcal/mol) seemed like unfavorable. It is agreed with kinetic results that the compound **2** simultaneously bind to CAS when interacting with the targets.

For **11** (Fig. 8B), Phe329 (−2.2 kcal/mol) seemed like the only important residue while Gly116 (0.22 kcal/mol) and His438 (0.02 kcal/mol) were seen as unfavorable. We speculated that the rigidity of the benzenesulfonyl group is too large. The formation of π-π T-shaped with Gly116 needed to overcome larger energy. Further modification can focus on increasing flexibility while maintaining the interaction with Gly116. The results showed that **11** was a competitive inhibitor which is inconsistent with kinetic result. We conclude that the conformation of **11** may be not the dominant conformation when bounding to protein. The specific explanation needs further research.

For **13** (Fig. 8C), Trp82 (−3.14 kcal/mol) and Phe329 (−1.42 kcal/mol) played a major role in binding free energy. And it was similar to compound **5**, Trp82 contributed more than Phe329. Therefore, compound **13** was a competitive inhibitor favoring competitive, either.

For **17** (Fig. 8D), Trp82 (−2.66 kcal/mol) Phe329 (−1.35 kcal/mol) and Tyr 332 (−1.88 kcal/mol) played a major role in binding free energy. And it was similar to compound **13**, Trp82 contributed mostly to the total binding free energies. Therefore, compound **17** was a competitive inhibitor.

The result of energy decomposition of potential hot residues demonstrated that van der Waals energy is important and polar solvation energy is adverse for all four compounds. The effect of Electrostatic energy and non-polar solvation energy on binding free energy is limited.

2.7. Antiproliferative assay

To determine the potential cytotoxic effects of hit compounds on neuronal cell line SH-SY5Y, the cell viability was evaluated by 3-(4,5-dimethylthiazol-2-yl)-2,5-diphenyltetrazolium (MTT) assay [25]. In general, all tested showed similar effects on SH-SY5Y with weak or no toxicity at concentrations of 10 and 50 μM (Fig. 9) except compound **5**. Compound **5** was safe at the concentration of 10 μM (109.8 ± 2.9%), however it caused greater toxicity at the concentration of 50 μM

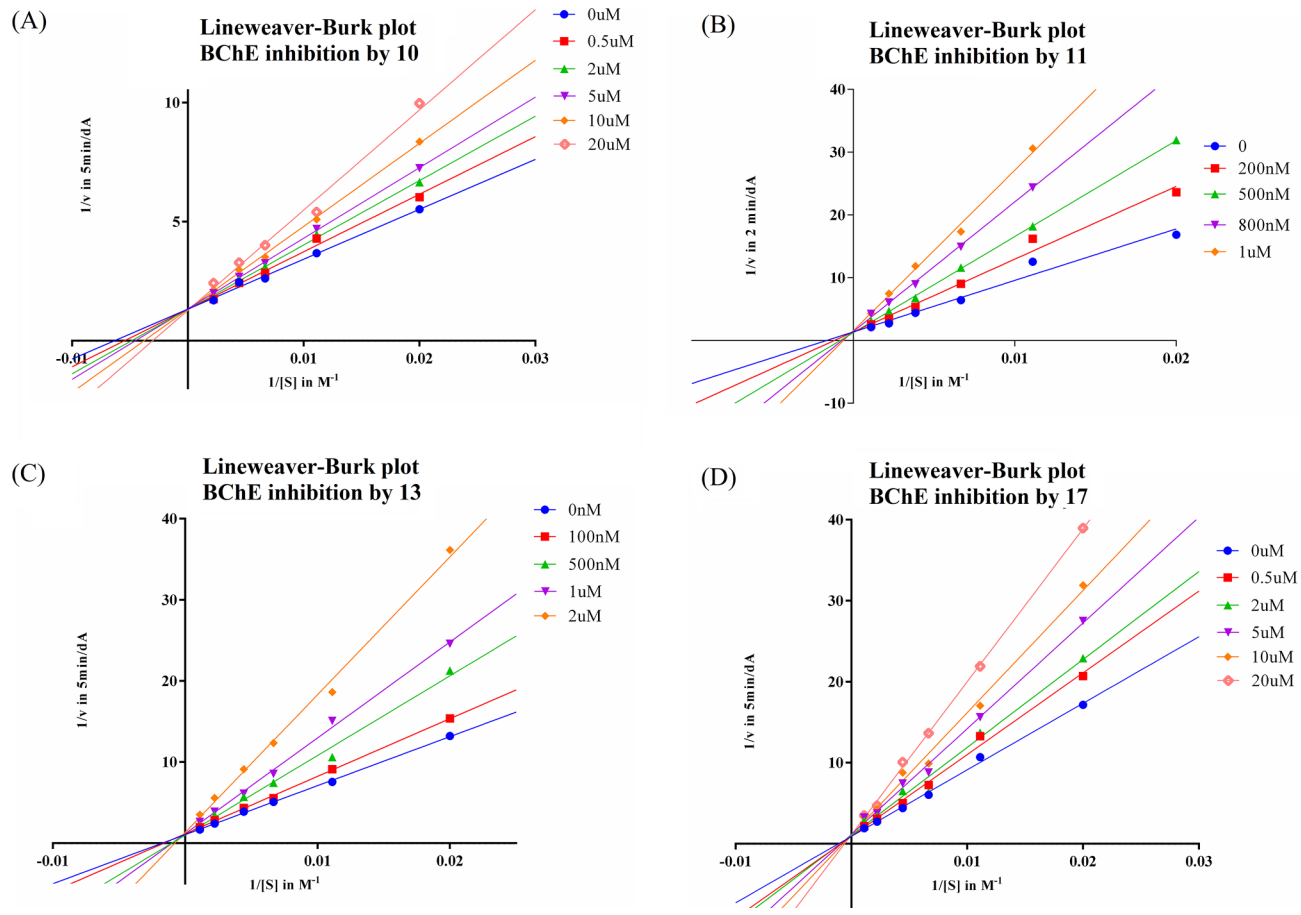

Fig. 6. Lineweaver-Burk plot of compound **10** (A), **11** (B), **13** (C), **17** (D) resulting from sub-velocity curves of BChE activity with different substrate concentrations (0.5–20 μM) in the absence and presence of the compounds with different concentrations.

Table 2
The inhibitory activities against ChEs of the hits from virtual screening.

Compound	ID number	AChE IR[a] (%)	BChE IR (%) or IC_{50} (μM)		
			IR[b] (%)	*eq*BChE	huBChE
2	Z16278154	26.2 ± 0.1	61.7 ± 0.3	0.6 ± 0.2	21.8 ± 70.0
3	Z19109045	19.2 ± 0.5	19.7 ± 2.5	nd[c]	nd
4	Z425617508	21.4 ± 0.7	17.5 ± 5.6	nd	nd
5	G396-0941	14.1 ± 1.0	84.3 ± 0.3	0.3 ± 0.1	9.3 ± 20.7
6	C036-0014	18.4 ± 0.8	19.0 ± 3.8	nd	nd
7	C036-1009	12.5 ± 0.4	4.0 ± 1.0	nd	nd
8	Z2654588491	19.5 ± 0.7	37.8 ± 0.3	nd	nd
9	C528-1247	8.6 ± 1.3	19.3 ± 2.8	nd	nd
10	Z57362660	18.7 ± 0.7	66.0 ± 0.3	2.2 ± 0.2	7.5 ± 5.0
11	C769-1472	22.5 ± 1.7	74.7 ± 0.6	0.7 ± 0.2	1.3 ± 0.6
12	C481-1228	16.0 ± 1.0	51.4 ± 1.3	13.5 ± 2.2	78.4 ± 100.1
13	Z343973836	11.8 ± 0.2	90.5 ± 0.5	0.7 ± 0.2	1.4 ± 1.9
14	Z105648980	11.8 ± 0.3	51.1 ± 2.0	7.3 ± 1.1	NA[d]
15	STOCK5S-92892	19.2 ± 0.1	24.52 ± 2.3	nd	nd
16	Z64830473	11.5 ± 0.5	8.4 ± 0.6	nd	nd
17	Z164597606	9.3 ± 0.4	61.9 ± 0.9	1.3 ± 0.3	1.7 ± 2.7
18	Z46480114	20.8 ± 0.7	14.6 ± 0.3	nd	nd
Tacrine		89.3 ± 0.1	91.9 ± 0.2	0.009 ± 0.002	0.003 ± 0.004

All data are shown as mean ± S.E.M. of three experiments.
[a] AChE (EC 3.1.1.7) from electric eel.
[b] BChE (EC 3.1.1.8) from horse serum.
[c] nd = not determined.
[d] NA = no active.

(11.0 ± 2.4%). More interestingly, six compounds showed better performance at concentration of 50 μM than 10 μM, especially compound **2** (10 μM: 99.5 ± 1.5%, 50 μM: 131.1 ± 1.8%), **10** (10 μM:121.8 ± 6.5%, 50 μM:161.3 ± 1.3%) and **17**(10 μM:108.0 ± 0.5%, 50 μM: 133.1 ± 4.8%). The results indicated that hit compounds except **5** showed preliminary safety on neuronal cell SH-SY5Y.

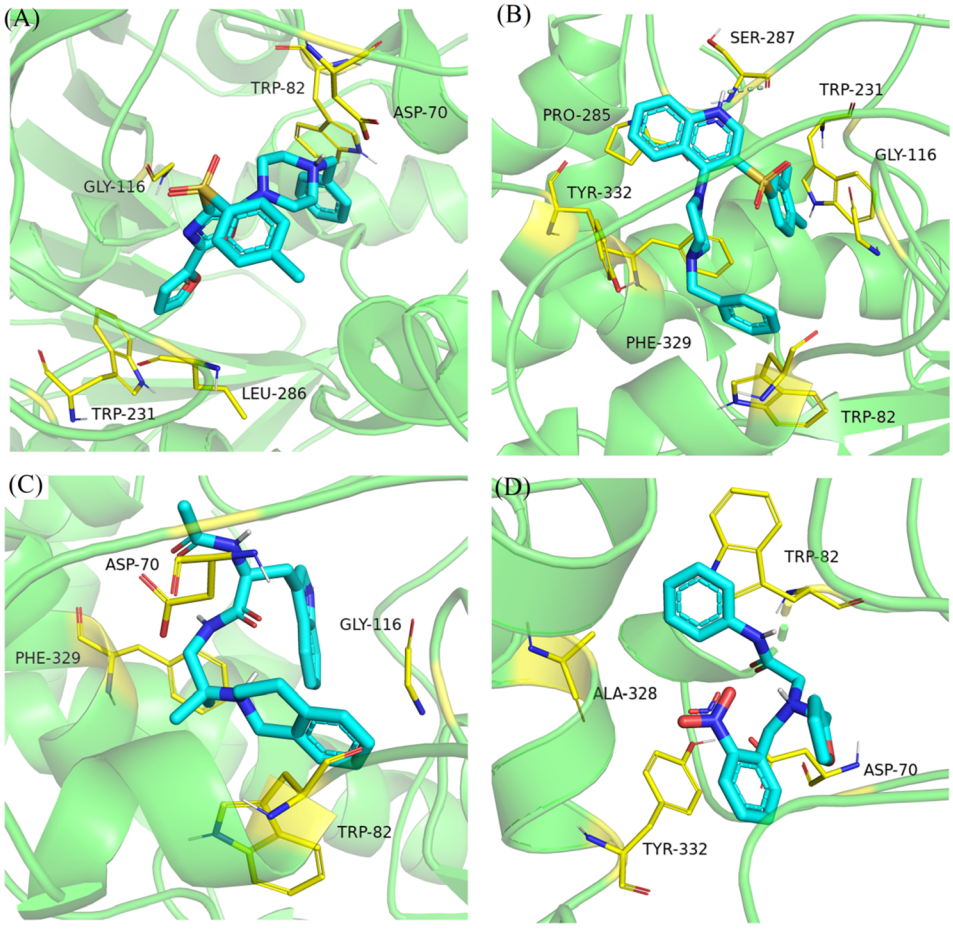

Fig. 7. Binding mode predictions for **10** (A), **11** (B), **13** (C), and **17** (D) with BChE (PDB ID: 5DYW). Compounds were shown in cyan stick mode; key residues were shown in yellow stick mode. Only polar hydrogen atoms were shown. H-bonds are represented by light green dotted lines.

Table 3
Predicted Free Energies (kcal/mol) for Binding of **2**, **5**, **11** or **13** to Human BChE by the MM/PBSA Method.

Energy terms (kcal/mol)	**10**	**11**	**13**	**17**
VDWAALS[a]	−52.13 ± 4.38	−53.23 ± 2.78	−46.50 ± 4.49	−41.74 ± 2.78
EEL[b]	−141.21 ± 19.62	−141.02 ± 13.43	−111.41 ± 17.87	−137.42 ± 9.67
EGB[c]	149.40 ± 16.06	147.32 ± 12.30	127.16 ± 17.93	155.53 ± 10.18
ESURF[d]	−6.50 ± 0.45	−6.06 ± 0.29	−554 ± 0.55	−5.12 ± 0.26
DELTA G gas[e]	−193.34 ± 19.85	−194.25 ± 14.45	−157.91 ± 20.74	−179.15 ± 10.29
DELTA G solv[f]	142.90 ± 16.13	141.26 ± 12.21	121.62 ± 17.61	150.11 ± 10.17
DELTA TOTAL[g]	−50.45 ± 8.24	−53.00 ± 4.77	−36.29 ± 5.29	−29.04 ± 3.40

[a] van der Waals energy.
[b] Electrostatic energy.
[c] Polar solvation energy.
[d] Non-polar solvation energy.
[e] Total gas phase free energy.
[f] Total solvation free energy.
[g] Total binding free energy.

2.8. ADMET in silico prediction

As shown in Table 4, all compounds appeared to have moderate or poor solubility in aqueous media and have high hydrophobicity, whereas it possessed good absorption except compound **5** and **11**. Fortunately, two compounds with better inhibitory activity (compound **5**, **11**) were predicted to have very high blood–brain barrier (BBB) penetration, which is a favoured property for the treatment of AD. Compounds with PSA-2D > 80 (**12**, **14**, **17**) are difficult to penetrate the BBB. Further modification can be done in consideration of decreasing PSA-2D to improve the BBB penetration. All compounds may not bind to CYP2D6, which would be beneficial for ensuring the efficacy of compounds and avoiding the potential side effect. All compounds may be highly bound to plasma proteins except compound **13**. In this prediction, however, most compound exhibit hepatotoxicity except (**2**, **5**, **13**), and further biological experiments are required to obtain additional data.

3. Conclusion

In the present study, we demonstrate the effectiveness of using a hierarchical structure-based virtual screening work owing to identify

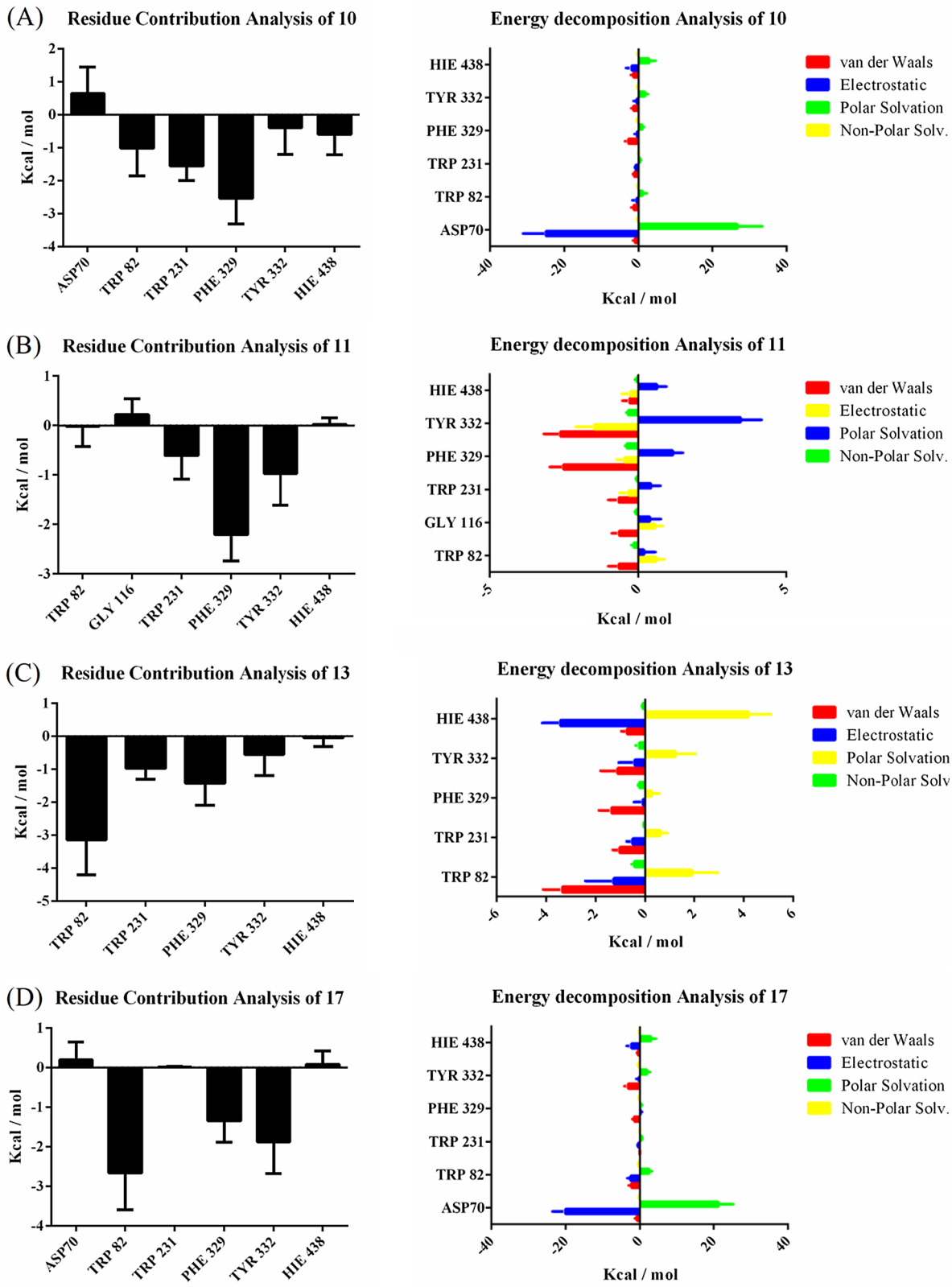

Fig. 8. Residue contributions of potential hot residues and energy decomposition of potential hot residues of **10**(A), **11**(B), **13**(C) and **17**(D); For all energies, unit is Kcal/mol.

new BChE inhibitors. Developed pharmacophore features were validated by ROC curves, and the best-performing model was selected for screening six commercial databases containing 3.9 million compounds. Molecules passed drug-like filters were further studied by docking and cluster. Compounds with good docking scores and showing structure diversity were evaluated for their *in vitro* enzyme inhibition activity. Among 17 compounds selected for bioassay, 8 of them exhibited the inhibition of < 20 μM on *eq*BChE and 7 showed IC_{50} < 100 μM on *hu*BChE. No compounds showed inhibition on AChE. The IC_{50} of three most active compounds (**11**, **13** and **17**) on *hu*BChE were 1.3 μM,

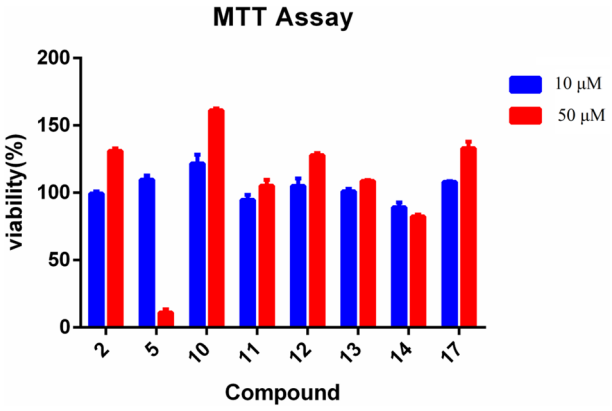

Fig. 9. The cytotoxicity of hit compounds on SH-SY5Y cells.

1.4 μM and 1.7 μM, respectively. All these compounds with diverse new scaffolds were selective BChE. The strategy we used in this study may have a wide application in further rational drug design. These compounds will no doubt provide a very good starting point for the discovery of highly selective BChE inhibitors.

4. Experimental section

4.1. Pharmacophore model generation

The 3D structure of the human BChE was downloaded from Protein Data Bank (PDB ID 5DYW) and imported into BIOVIA Discovery Studio 3.0 (DS, BIOVIA, San Diego, CA, USA). The protein was prepared within protein preparation module as the basis of pharmacophore generation and docking. The pharmacophore models were constructed using the Receptor-Ligand Pharmacophore Generation protocol of DS. The parameters for pharmacophore generation were set as follows: Minimum Features 4, Maximum Features 6. Other parameters were set as default. The exclusion volume was added to the pharmacophore model as default.

To evaluate the performance of the model, a dataset contained actives and decoys was prepared. The Decoy-Finder was used to generate a set of decoys starting from 10 active compounds. The protocol generated 36 decoys from Zinc database for each active. The parameters for pharmacophore generation were set as follows: conformation generation: fast; Maximum Conformations: 100; fitting method: rigid. Other parameters were set as default. Receiving Operator Curve (ROC) was employed to assess the quality of models.

4.2. Virtual screening

For the pharmacophore model, virtual screenings were performed based on the query fit. The 3D database of six commercial databases was prepared using the Build 3D Database module. Align Ligand was set to True, and Search Method was set to Best. Other parameters were set as default. The hits from the pharmacophore screening were filtered by filtered by property module. The druglike filter was performed with the Filter by Lipinski and Veber rules module in DS. Docking stimulation was performed with the CDOCKER module implemented in DS. The protein used for pharmacophore generation was used here. The binding sites were defined as a site sphere (in 10 Å radius) around the native ligand. Other parameters were maintained as the defaults. Cluster Ligand with DS was used to cluster ligand. The number of cluster was set as 10 and the predefined set was FCFP_6. Other parameters were maintained as the defaults. Finally, 17 hits were purchased from Topscience (www.tsbiochem.com), with purity > 95% (liquid chromatography-mass spectrometry, LC-MS).

4.3. Biological evaluation

The assay followed the method of Ellman *et al.*, using a Thermo Fisher Scientific spectrophotometer. AChE (EC 3.1.1.7, Type VI-S, from Electric Eel, C3389), BChE (EC 3.1.1.8, from equine serum, C0663), BChE (EC 3.1.1.8, from human serum), 5,50-dithiobis (2-nitrobenzoic acid) (DTNB, D218200), acetylthiocholine iodide (ATC, A5751), and butyrylthiocholine iodide (BTC, B3253) were purchased from SigmaAldrich (St. Louis, MO, USA).

The test compounds were dissolved in dimethyl sulfoxide to stock. For each compound, a dilution series of six different concentrations (10^{-4} to 10^{-9} M) were prepared. For measurement, a cuvette containing 3.0 mL of phosphate buffer, 100 μL of AChE or BChE, and 100 μL of the test compound solution was allowed to stand for 5 min before 100 μL of DTNB were added. After the addition of 20 μL of ATC or BTC, the reaction was initiated and the solution was mixed immediately. Two minutes after substrate addition, the absorption was determined at 25 °C at 412 nm by Thermo Fisher Scientific spectrophotometer. 100 μL of water replaced the enzyme solution were used to determine the blank value. All measurement was performed in triplicate in parallel. The inhibition curve was drawn by plotting the percentage enzyme activity

Table 4
Predicted pharmacokinetic properties of hits.

Comp.	AlogP98[a]	PSA-2D[b]	Solubility Level[c]	Absorption Level[d]	BBB Level[e]	PPB[f]	CYP2D6[g]	Hepatotoxic[h]
2	5.216	55.629	2	0	1	true	false	false
5	3.316	56.274	1	1	0	true	false	true
10	5.003	77.767	1	0	1	true	false	false
11	5.794	52.567	1	1	0	true	false	true
12	3.751	103.397	2	0	4	true	false	true
13	3.146	78.629	2	0	2	false	false	false
14	3.18	96.526	3	0	3	true	false	true
17	3.199	88.84	2	0	3	true	false	true

[a] AlogP98: Lipophilicity descriptor.
[b] PSA-2D: Polar surface area.
[c] Solubility Level: (0, good; 1, moderate; 2, poor; 3, very poor).
[d] Absorption Level: (0, good; 1, moderate; 2, poor; 3, very poor).
[e] BBB Level: (0, very high blood–brain barrier penetration; 1, high; 2, medium; 3, low).
[f] PPB Prediction: The classification describing whether a compound is highly bound (> = 90% bound) to plasma proteins using the cutoff Bayesian score of −2.209 (obtained by minimizing the total number of false positives and false negatives).
[g] CYP2D6 Prediction: The classification describing whether a compound is a CYP2D6 inhibitor using the cutoff Bayesian score of 0.161 (obtained by minimizing the total number of false positives and false negatives).
[h] Hepatotoxic Prediction: The classification describing whether a compound is hepatotoxic using the cutoff Bayesian score of −4.154 (obtained by minimizing the total number of false positives and false negatives).

(100% for the reference) versus the logarithm of the test compound concentration. The IC_{50} values were calculated by GraphPad Prism 6, and the data were shown as mean ± SEM.

4.4. Kinetic study

Kinetic studies were performed in the same manner as the determination of ChE inhibition. For **10** and **17**, the substrate (BTC) was used in concentrations of 0.5, 2, 5, 10 and 20 μM. For **11**, the concentrations were set to 200, 500, 800, and 1000 nM. For **13**, the substrate (BTC) was used in concentrations of 100, 500, 1000, and 2000 nM. The enzymatic reaction was extended to 4 min before detecting the absorption. Linear regression was used to plot the Lineweaver-Burk plots using GraphPad Prism 6.

4.5. Molecular dynamics

MD simulations were performed using the PMEMD module in AMBER 16 accelerated by GPU system consist of the NVIDIA CUDA processor. [26] The initial docking poses of **2**, **5**, **11** and **13** bound with BChE were imported, respectively. The proteins were assigned with the AMBER ff99SB force field while the ligands were treated with the ANTECHAMBER module and the general AMBER force field [27,28]. All hydrogen atoms of the proteins and ligands were added using the Reduce Module. The systems were solvated in a TIP3P water box in a 9 Å hexahedron. Sodium ions were added with the purpose of neutralizing the systems. To remove possible steric stresses, the systems were minimized for 1,000 steps with the steepest descent method, followed by application of conjugate gradients for another 1,000 steps. All two systems were linearly heated from 0 to 300 K using a Langevin thermostat and weak restraints 10 kcal/mol on the protein backbone atoms over 1 ns. Finally, dynamics simulation of 20 ns NPT ensemble was set at 1 atm and 300 K. After MD simulation, 2000 frames were extracted from the 20 ns of trajectory for CPPTRAJ analysis [29]. The MMGBSA method in the AMBER 16 was used to calculate the binding free energies and energy decomposition [30].

4.6. MTT

SH-SY5Y cells (5×10^3, volume 0.1 mL) were placed in a 96-well flat-bottomed plate, and the cells were adhered to the bottom of the plate at 37° C overnight. Various concentrations of compounds were treated on cells for 24 h. MTT reagent was added to the wells and the plates were incubated for 4 h at 37 °C. The cells were disrupted by the addition of 0.1 mL of lysis buffer to the wells. After incubation, they were kept at 37° C for an additional 24 h, and the color reaction was measured at 492 nm using a spectrophotometer.

4.7. ADMET in silico prediction

The ADMET properties (absorption, distribution, metabolism, excretion, and toxicity) and physicochemical properties of were calculated within ADMET software and Calculate Molecular Properties in DS 3.0

Acknowledgement

We gratefully thank the support from the grants (Nos. 81872728, 81573281, 81803367 and 81830105) of National Natural Science Foundation of China. We also thank the support from Double First-Class“ initiative Innovation team project of China Pharmaceutical University (Nos. CPU2018GF11 and CPU2018GY34).

Appendix A. Supplementary material

Supplementary data to this article can be found online at https://doi.org/10.1016/j.bioorg.2018.12.023.

References

[1] C.A. Lane, J. Hardy, J.M. Schott, Alzheimer's disease, Eur. J. Neurol. 25 (2018) 59–70.
[2] K. Blennow, M.J. de Leon, H. Zetterberg, Alzheimer's disease, The Lancet 368 (2006) 387–403.
[3] P. Zis, A. Strydom, Clinical aspects and biomarkers of Alzheimer's disease in Down syndrome, Free Radic. Biol. Med. 114 (2018) 3–9.
[4] A. Bicer, P. Taslimi, G. Yakali, I. Gulcin, M. Serdar Gultekin, G. Turgut Cin, Synthesis, characterization, crystal structure of novel bis-thiomethylcyclohexanone derivatives and their inhibitory properties against some metabolic enzymes, Bioorg. Chem 82 (2018) 393–404.
[5] M. Zengin, H. Genc, P. Taslimi, A. Kestane, E. Guclu, A. Ogutlu, O. Karabay, I. Gulcin, Novel thymol bearing oxypropanolamine derivatives as potent some metabolic enzyme inhibitors - Their antidiabetic, anticholinergic and antibacterial potentials, Bioorg. Chem. 81 (2018) 119–126.
[6] A. Akincioglu, E. Kocaman, H. Akincioglu, R.E. Salmas, S. Durdagi, I. Gulcin, C.T. Supuran, S. Goksu, The synthesis of novel sulfamides derived from beta-benzylphenethylamines as acetylcholinesterase, butyrylcholinesterase and carbonic anhydrase enzymes inhibitors, Bioorg. Chem. 74 (2017) 238–250.
[7] R.M. Lane, S.G. Potkin, A. Enz, Targeting acetylcholinesterase and butyrylcholinesterase in dementia, Int. J. Neuropsychopharmacol. 9 (2006) 101–124.
[8] H.W. Klafki, M. Staufenbiel, J. Kornhuber, J. Wiltfang, Therapeutic approaches to Alzheimer's disease, Brain 129 (2006) 2840–2855.
[9] Y. Chen, H. Lin, H. Yang, R. Tan, Y. Bian, T. Fu, W. Li, L. Wu, Y. Pei, H. Sun, Discovery of new acetylcholinesterase and butyrylcholinesterase inhibitors through structure-based virtual screening, RSC Adv. 7 (2017) 3429–3438.
[10] V. Andrisano, M. Naldi, A. De Simone, M. Bartolini, A patent review of butyrylcholinesterase inhibitors and reactivators 2010–2017, Expert Opin. Ther. Pat. 28 (2018) 455–465.
[11] B. Li, E.G. Duysen, M. Carlson, O. Lockridge, The butyrylcholinesterase knockout mouse as a model for human butyrylcholinesterase deficiency, J. Pharmacol. Exp. Ther. 324 (2008) 1146–1154.
[12] N.H. Greig, T. Utsuki, D.K. Ingram, Y. Wang, G. Pepeu, C. Scali, Q.S. Yu, J. Mamczarz, H.W. Holloway, T. Giordano, D. Chen, K. Furukawa, K. Sambamurti, A. Brossi, D.K. Lahiri, Selective butyrylcholinesterase inhibition elevates brain acetylcholine, augments learning and lowers Alzheimer beta-amyloid peptide in rodent, in: Proceedings of the National Academy of Sciences of the United States of America, 102 (2005) 17213-17218.
[13] S. Darvesh, M.K. Cash, G.A. Reid, E. Martin, A. Mitnitski, C. Geula, Butyrylcholinesterase is associated with beta-amyloid plaques in the transgenic APPSWE/PSEN1dE9 mouse model of Alzheimer disease, J. Neuropathol. Exp. Neurol. 71 (2012) 2–14.
[14] Y. Furukawa-Hibi, T. Alkam, A. Nitta, A. Matsuyama, H. Mizoguchi, K. Suzuki, S. Moussaoui, Q.S. Yu, N.H. Greig, T. Nagai, K. Yamada, Butyrylcholinesterase inhibitors ameliorate cognitive dysfunction induced by amyloid-beta peptide in mice, Behav. Brain Res. 225 (2011) 222–229.
[15] Gohar Mushtaq, Nigel H. Greig, Jalaluddin A. Khan, M.A. Kamal, Status of acetylcholinesterase and butyrylcholinesterase in Alzheimer's disease and Type 2 diabetes mellitus, CNS Neurol. Disord. Drug Targets 13 (2014) 1432–1439.
[16] I.R. Macdonald, S.P. Maxwell, G.A. Reid, M.K. Cash, D.R. DeBay, S. Darvesh, Quantification of butyrylcholinesterase activity as a sensitive and specific biomarker of Alzheimer's disease, J. Alzheimer's Disease : JAD 58 (2017) 491–505.
[17] P.W. Elsinghorst, C.M. Tanarro, M. Gutschow, Novel heterobivalent tacrine derivatives as cholinesterase inhibitors with notable selectivity toward butyrylcholinesterase, J. Med. Chem. 49 (2006) 7540–7544.
[18] S. Rizzo, C. Riviere, L. Piazzi, A. Bisi, S. Gobbi, M. Bartolini, V. Andrisano, F. Morroni, A. Tarozzi, J.P. Monti, A. Rampa, Benzofuran-based hybrid compounds for the inhibition of cholinesterase activity, beta amyloid aggregation, and abeta neurotoxicity, J. Med. Chem. 51 (2008) 2883–2886.
[19] C.G. Carolan, G.P. Dillon, J.M. Gaynor, S. Reidy, S.A. Ryder, D. Khan, J.F. Marquez, J.F. Gilmer, Isosorbide-2-carbamate esters: potent and selective butyrylcholinesterase inhibitors, J. Med. Chem. 51 (2008) 6400–6409.
[20] Q. Yu, H.W. Holloway, T. Utsuki, A. Brossi, N.H. Greig, Synthesis of novel phenserine-based-selective inhibitors of butyrylcholinesterase for Alzheimer's disease, J. Med. Chem. 42 (1999) 1855–1861.
[21] U. Kosak, B. Brus, D. Knez, S. Zakelj, J. Trontelj, A. Pislar, R. Sink, M. Jukic, M. Zivin, A. Podkowa, F. Nachon, X. Brazzolotto, J. Stojan, J. Kos, N. Coquelle, K. Salat, J.P. Colletier, S. Gobec, The magic of crystal structure-based inhibitor optimization: development of a butyrylcholinesterase inhibitor with picomolar affinity and in vivo activity, J. Med. Chem. 61 (2018) 119–139.
[22] A. Cereto-Massague, L. Guasch, C. Valls, M. Mulero, G. Pujadas, S. Garcia-Vallve, DecoyFinder: an easy-to-use python GUI application for building target-specific decoy sets, Bioinformatics 28 (2012) 1661–1662.
[23] X. Lu, H. Yang, Y. Chen, Q. Li, S.Y. He, X. Jiang, F. Feng, W. Qu, H. Sun, The development of pharmacophore modeling: generation and recent applications in drug discovery, Curr. Pharm. Des. (2018).
[24] C. Zhang, L.J. Feng, Y. Huang, D. Wu, Z. Li, Q. Zhou, Y. Wu, H.B. Luo, Discovery of novel phosphodiesterase-2A inhibitors by structure-based virtual screening structural optimization, and bioassay, J. Chem. Inform. Model. 57 (2017) 355–364.
[25] M. Tugrak, H. Inci Gul, H. Sakagami, I. Gulcin, C.T. Supuran, New azafluorenones with cytotoxic and carbonic anhydrase inhibitory properties: 2-Aryl-4-(4-hydroxyphenyl)-5H-indeno[1,2-b]pyridin-5-ones, Bioorg. Chem. 81 (2018) 433–439.
[26] D.A. Case, R.M. Betz, D.S. Cerutti, T.E. Cheatham III, T.A. Darden, R.E. Duke, T.J. Giese, H. Gohlke, A.W. Goetz, N. Homeyer, S. Izadi, P. Janowski, J. Kaus,

A. Kovalenko, T.S. Lee, S. LeGrand, P. Li, C. Lin, T. Luchko, R. Luo, B. Madej, D. Mermelstein, K.M. Merz, G. Monard, H. Nguyen, H.T. Nguyen, I. Omelyan, A. Onufriev, D.R. Roe, A. Roitberg, C. Sagui, C.L. Simmerling, W.M. Botello-Smith, J. Swails, R.C. Walker, J. Wang, R.M. Wolf, X. Wu, L. Xiao, P.A. Kollman, AMBER 2016, University of California, San Francisco, 2016.

[27] V. Hornak, R. Abel, A. Okur, B. Strockbine, A. Roitberg, C. Simmerling, Comparison of multiple Amber force fields and development of improved protein backbone parameters, Proteins 65 (2006) 712–725.

[28] W. Zhang, T.J. Hou, X.B. Qiao, X.J. Xu, Parameters for the generalized born model consistent with RESP atomic partial charge assignment protocol, J. Phys. Chem. B 107 (2003) 9071–9078.

[29] D.R. Roe, T.E. Cheatham 3rd, PTRAJ and CPPTRAJ: software for processing and analysis of molecular dynamics trajectory data, J. Chem. Theory Comput. 9 (2013) 3084–3095.

[30] B.R. Miller 3rd, T.D. McGee Jr., J.M. Swails, N. Homeyer, H. Gohlke, A.E. Roitberg, MMPBSA.py: an efficient program for end-state free energy calculations, J. Chem. Theory Comput. 8 (2012) 3314–3321.